Physics Letters B 748 (2015) 178–182

Contents lists available at ScienceDirect

Physics Letters B

www.elsevier.com/locate/physletb

Toward a reassessment of the $^{19}F(p,\alpha_0)^{16}O$ reaction rate at astrophysical temperatures

I. Lombardo [a,b,*], D. Dell'Aquila [a,b], A. Di Leva [a,b], I. Indelicato [c,d], M. La Cognata [d], M. La Commara [a,b], A. Ordine [b], V. Rigato [e], M. Romoli [b], E. Rosato [a,b,1], G. Spadaccini [a,b], C. Spitaleri [c,d], A. Tumino [d,f], M. Vigilante [a,b]

[a] Dip. di Fisica, Univ. di Napoli Federico II, via Cintia, Napoli, Italy
[b] INFN – Sezione di Napoli, via Cintia, Napoli, Italy
[c] Dip. di Fisica e Astronomia, Univ. di Catania, via S. Sofia, Catania, Italy
[d] INFN – Laboratori Nazionali del Sud, via S. Sofia, Catania, Italy
[e] INFN – Laboratori Nazionali di Legnaro, Legnaro (Padova), Italy
[f] Fac. di Ingegneria e Architettura, Univ. Kore di Enna, Enna, Italy

ARTICLE INFO

Article history:
Received 30 October 2014
Received in revised form 30 May 2015
Accepted 29 June 2015
Available online 2 July 2015
Editor: V. Metag

Keywords:
Nuclear reactions
Fluorine nucleosynthesis

ABSTRACT

The $^{19}F(p,\alpha_0)^{16}O$ reaction at low energies plays an important role in fundamental physics. In particular in nuclear astrophysics it represents, together with the $^{19}F(p,\gamma)^{20}Ne$ reaction, the crossing point between the CNO and the NeNa cycles in stars. Further, in hydrogen-rich stellar environments, it is the most important fluorine destruction channel. In this paper we report new measurements on the $^{19}F(p,\alpha_0)^{16}O$ reaction at deeply sub-Coulomb energies (0.2–0.6 MeV), a region where, despite the key role of this reaction, very few and old data are reported. The deduced astrophysical S-factor is ≈1.5–2 times larger than currently adopted extrapolations with possibly important astrophysical consequences.

1. Introduction

The transmutation of ^{19}F induced by low energy protons has attracted noticeable interest since the beginning of Nuclear Physics [1–5]. The emission of long range α particles was early recognized [2] and was ascribed to a large exoergic nuclear reaction ($Q = 8.114$ MeV, [6]), the $^{19}F(p,\alpha_0)^{16}O$ one. The analysis of this reaction, together with the pair-emitting one $^{19}F(p,\alpha_\pi)^{16}O^*$ ($E_x = 6.05$ MeV), allowed to study the spectroscopy of natural-parity states in the self-conjugated compound nucleus ^{20}Ne, in a large range of excitation energy, from $E_x \simeq 13.23$ MeV up to $E_x \simeq 18.43$ MeV. This energy domain lays between two important disintegration energy values of ^{20}Ne: the 11.89 MeV $^{12}C+2\alpha$ threshold and the 19.17 MeV 5α threshold [6,7]. As pointed out in various theoretical works (see, e.g., [7,8]), α-cluster effects in self-conjugated nuclei have been predicted to arise near the Nα disintegration thresholds. Therefore, these reactions are a tool well suited to investigate the α-cluster structure of ^{20}Ne. Results of spectroscopic investigations are reported, e.g., in [6,9–14]. Another important feature stimulating the investigation of the $^{19}F(p,\alpha_0)^{16}O$ reaction at energies far below the Coulomb barrier is certainly related to its astrophysical importance [15]. In massive stars the competition between $^{19}F(p,\gamma)^{20}Ne$ and $^{19}F(p,\alpha)^{16}O$ in the hydrogen burning phase determines the quantity of catalytic material that is lost in the CNO cycle and becomes available for the NeNa one [15–17]. Despite its importance, the S-factors and the branching ratio between the α_0, α_π and α_γ outgoing channels in the $^{19}F(p,\alpha)^{16}O$ reaction are still largely uncertain at astrophysical energies [18], pointing out the need for new, more comprehensive, measurements. The most recent experimental work on this subject is Ref. [17], suggesting that at the lowermost energies ($T < 0.1$ GK) the α_0 channel dominates in the other open reaction channels (i.e. α_π, α_γ). Furthermore, fluorine nucleosynthesis is an open issue of modern astrophysics, and it has been suggested that $^{19}F(p,\alpha)^{16}O$ reactions can play an important role in hydrogen-rich environments [19–21]. Nowadays, the Asymptotic Giant Branch (AGB) stars are believed to be the main sites of fluorine production [19]. In particular, in the case of thermally-pulsing AGB stars, extra-mixing of material through the zone of radiative energy transport above

* Corresponding author.
E-mail address: ivlombardo@na.infn.it (I. Lombardo).
[1] Deceased.

http://dx.doi.org/10.1016/j.physletb.2015.06.073

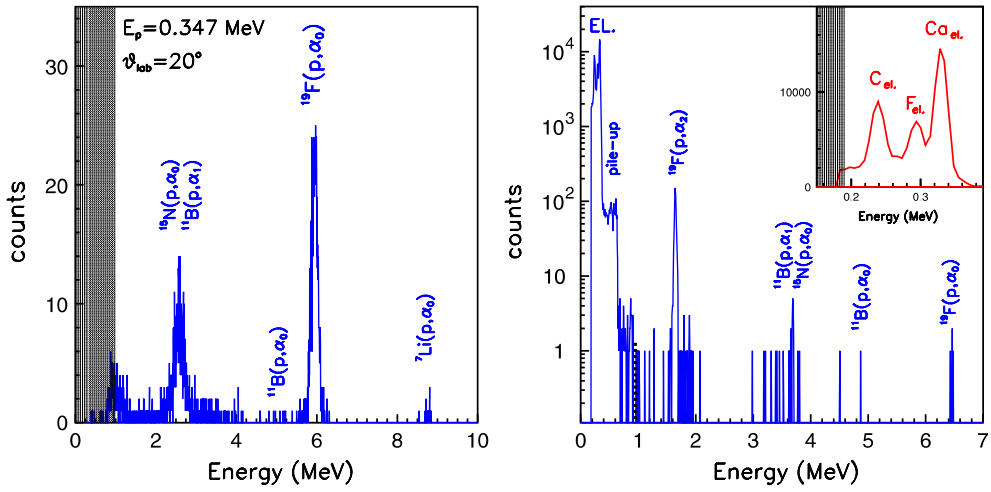

Fig. 1. (Color online.) (Left panel) Experimental spectrum at $\theta_{lab} = 20°$ and $E_p = 0.347$ MeV with the Al absorber. Kinematics and energy loss considerations allow to identify the peaks due to the various reactions. (Right Panel) Experimental spectrum obtained at $\theta_{lab} = 160°$ and $E_p = 0.347$ MeV by using a tightly collimated unshielded silicon detector. For clarity, the elastic peak and the pile-up region is scaled by a ≈500 factor. A magnified view of elastic scattering peaks is reported in the insert. The shadow region indicates electronic threshold.

the hydrogen shell (often referred to as *deep mixing* or *cool bottom processing* phenomena) can occur [22]. This may lead to important alteration of the isotopic composition of stellar outer layers [20]. The mixing process can expose material at temperatures high enough to activate the ^{19}F(p,α)^{16}O reaction [21,23], becoming an important fluorine destruction channel [19]. The accurate knowledge of the ^{19}F(p,α)^{16}O reaction rate around the AGB Gamow window ($E_{cm} \approx 27$–94 keV at $T \simeq 0.04$ GK) is therefore of crucial importance for modeling nucleosynthesis in these stars [20] and may help to solve large discrepancies between stellar model predictions and experimental observations [19].

Despite its astrophysical relevance, the behavior of the ^{19}F(p,α_0)^{16}O astrophysical S-factor is largely uncertain, especially at low energies, as early noted by [24,25]. The Nuclear Astrophysics Compilation of Reaction Rates (NACRE) [18] extrapolated the S-factor from direct data available in the literature in the $E_{cm} = 0.46$–2.54 MeV energy domain [5,9–12]. At lower energies, unpublished data [26] referred in [27,28] exist, and were not included in the NACRE compilation as possibly affected by normalization problems [18]. More recently, two experimental works have been reported. The first one explores the low energy region by using the Trojan Horse Method THM [20,29]. The authors argue the possible existence of resonances leading to a significant increase of the reaction rate at energies of stellar interest [20]. The second one is a direct measurement carried out in the energy range $E_{cm} = 0.577$–0.982 MeV [14], that partially covers the lowermost energy data by Breuer [10]. In that work a good agreement with Breuer [10] and Caracciolo et al. [11] direct data was observed [14] suggesting that the non-resonant part of the S-factor at low energies might be larger than the NACRE extrapolation.

In this Letter we report a direct experimental measurement of ^{19}F(p,α_0)^{16}O S-factor in the $E_{cm} = 0.18$–0.60 MeV range, exploring a low-energy region where, to our knowledge, no direct experimental data have been published. The lowermost energy region of the new experimental data set is close to the upper limit of the Gamow window at $T = 0.04$ GK, and partially covers the $E_{cm} \approx 50$–300 keV energy interval needed for accurate modeling of the nucleosynthesis scenarios in post-AGB stars [20]. The experimental results point out the existence of several resonances, and an R-matrix fit of the data allows to determine the contribution given by each ^{20}Ne state to the S-factor. The resulting reaction rate estimate is significantly larger than NACRE [18].

2. Experimental details

The experiment was performed at the AN2000 Van de Graaf accelerator of Laboratori Nazionali di Legnaro (Padua, Italy). The energy calibration of the proton beam was determined by measuring with a $LaBr_3$(Ce) crystal the γ-ray yield of the ^{19}F(p,$\alpha\gamma$)^{16}O reaction around the resonance at 340 keV, and by using a previous calibration point obtained by studying the γ-ray yield of the ^{27}Al(p,γ)^{28}Si reaction around the resonance at 992 keV. This calibration has been frequently checked during the experiment and further benchmarked by considering the position of 0.484, 0.594 and 0.669 keV resonances in the yield curve of the α_2 line (associated with the 6.13 MeV state in ^{16}O) measured with a silicon detector at $\theta_{lab} = 160°$. A further check was the shape analysis of the dip in the elastic scattering differential cross sections ^{12}C(p,p$_0$)^{12}C at $\theta_{lab} = 160°$ in the $E_p = 450$ keV region. The two methods give consistent results within ≈1 keV. From the measured width of the 340 keV resonance ($\Gamma = 2.4$ keV [6]) in the ^{19}F(p,α_2)^{16}O yield it is possible to estimate a beam energy resolution of $\approx \pm 2.5$ keV.

In this experiment, the proton beam intensity ranged from 0.3 to 0.9 μA. The target consisted of a CaF_2 layer (30 μg/cm^2 thick) evaporated onto a natural carbon backing (20 μg/cm^2 thick) and was frequently changed to avoid degradation.

Target thickness was determined during evaporation by means of the resonating quartz method and was subsequently cross-checked by means of elastic backscattering analysis with proton beams at several energies; the resulting overall accuracy is ≈3%. Target stability was checked all along the experiment by repeated measurements at the same energy. The elastic backscattering spectra indicate a natural stoichiometric ratio of the CaF_2 layer, in agreement with [16,30]. The effect of target thickness has been carefully taken into account according to the procedure outlined in Ref. [15]. The detection system consisted of 12 silicon detectors mounted at various polar angles and placed at 10–12 cm from the target centre. The detectors, 300 μm thick, have 1×1 cm^2 active area. A thin aluminium absorber (8 μm thick) was placed in front of the silicon detectors in order to suppress scattered protons [9,14].

In the left panel of Fig. 1 we show the spectrum obtained with a silicon detector covered by the Al absorber at $E_p = 0.347$ MeV and $\theta_{lab} = 20°$. A very low background is seen for the ^{19}F(p,α_0)^{16}O peaks in the bombarding energy domain here investigated. Peaks

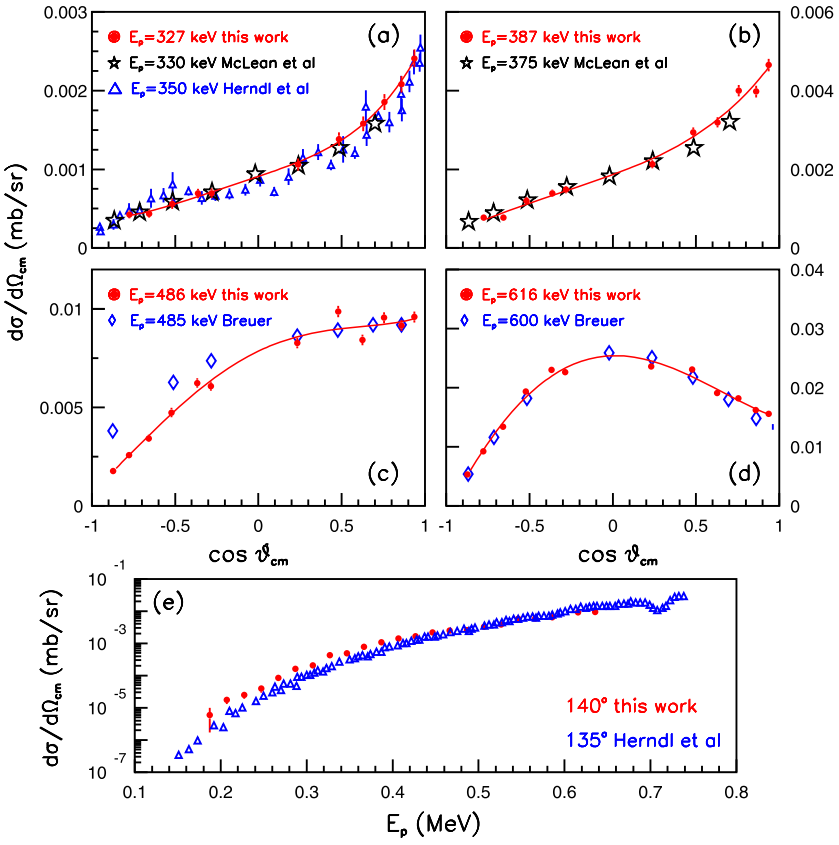

Fig. 2. (Color online.) (Panels a–d) Angular distributions of the ^{19}F(p,α_0)^{16}O reaction at $E_p = 0.327$, 0.387, 0.486 and 0.616 MeV. Red dots: Present data. Red lines: Legendre polynomial fits. Black stars: data from Ref. [4]. Blue diamonds: data from Ref. [10]. Blue triangles: data from Ref. [26]. Data from Refs. [4,10,26] have been normalized to our cross section scale as discussed in the text. (e) Excitation function obtained in this experiment at 140° (red dots) compared with data reported at 135° in Ref. [27] (blue triangles).

due to reactions on the main target contaminants are indicated in the figure. In particular, no appreciable contamination is due to the close-lying ^{11}B(p,α_0)^{8}Be reaction. In this case, indeed, the energy resolution of experimental spectra (≈0.2 MeV FWHM) is larger than the energy separation of the ^{11}B(p,α_0)^{8}Be and ^{19}F(p,α_0)^{16}O peaks at all angles and bombarding energies (≈0.7 MeV in the worst case).

The angular resolution was estimated to be $\simeq 2.8°$, as in Ref. [9]. Solid angles were determined by geometry with an accuracy better than 3%. Beam current was measured by means of a Faraday cup placed behind the target and a −300 V suppression voltage was applied to reduce secondary electron effects. A copper rod cooled to liquid nitrogen temperature was placed inside the scattering chamber in order to reduce carbon build up effects. The reaction chamber was operated under high vacuum condition (better than 10^{-6} mbar).

As already mentioned, a tightly collimated (≈4 mm^2) detector was placed at $\theta_{lab} = 160°$ to detect backscattered protons. In the right panel of Fig. 1 we show a spectrum obtained with this silicon detector at $E_p = 0.347$ MeV bombarding energy. In this way it was possible to make a check of the absolute cross section scale for several bombarding energies. In fact, at low energies, the p+Ca elastic scattering cross section can be theoretically predicted [31]. The analysis of the p+Ca elastic backscattering peak at various energies (including low energy points in the 0.25–0.35 MeV domain) leads to elastic cross section estimates in agreement with Rutherford predictions (taking into account electron screening effects, of the order of 1% [31]) within ≈7%; this number can be assumed as the maximum overall non-statistical error on the absolute cross section scale.

3. Angular distributions and *S*-factor

Fig. 2 (panels a–d) displays present experimental angular distributions (red dots) together with data available from the literature. In the $E_p \approx 0.3$–0.4 MeV interval only the very old data (in arbitrary units) by McLean, Ellett and Jacobs [4] exist. Here, they have been normalized to our cross section and shown for comparison in Fig. 2(a,b). The shapes of these angular distributions are in good agreement with our results. In the same energy region, unpublished results by Lorenz-Wirzba [26] have been quoted in Refs. [27,28]. These data at $E_p = 0.35$ MeV have been normalized (by a factor of 2) to our cross section scale and are shown as blue triangles in Fig. 2a. A good agreement between the shapes of angular distributions is observed. In Ref. [18] it was hypothesized that the cross section values of the low energy part of this data set could be underestimated. In Fig. 2e we show a comparison of the excitation functions at 140° and 135° from the present measurements and data from Refs. [26,27], respectively. A reasonable agreement is seen at $E_p > 0.4$ MeV, while at low energies the cross section data from Refs. [26,27] have a different slope. It is interesting to note that discrepancies respect to the cross section data of Ref. [26] have been reported also by other authors in unpublished works, as reported in the review paper [25]. Fig. 2(c,d) show the angular distributions obtained at $E_p = 0.482$ and 0.612 MeV, together with the data by Breuer [10] normalized to our cross section scale. The agreement between the two data sets is quite good.

A strong forward–backward asymmetry of the angular distributions is seen in the $E_p = 0.2$–0.5 MeV region. This effect can be explained in two different ways. It can be attributed to in-

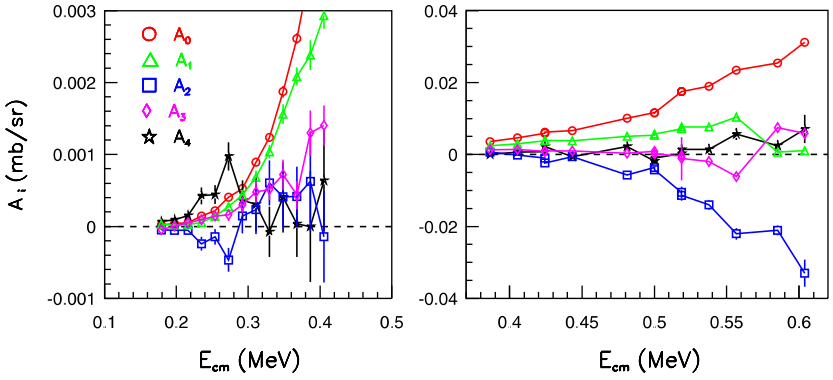

Fig. 3. (Color online.) Evolution with the energy of the A_i coefficients of cosine power fit of experimental angular distributions obtained in the present experiment. Error bars are statistical. Note the change of vertical scale in the left and right panels.

terference effects between opposite parity close-lying resonances [9–11] or to the onset of direct processes at sub-Coulomb energies, possibly triggered by cluster structures in the ^{19}F target nucleus [27,28,32]. To investigate these aspects we analyze angular distributions in terms of cosine polynomials [9,11]. The trend of the A_i coefficients deduced from the fit of experimental data (truncated to the 4th order) is reported in Fig. 3 (left and right panels). The smooth behavior of the A_0 and A_2 terms in the $E_p = 0.3$–0.5 MeV region can be mainly due to direct processes, while the broad bump of the A_4 term in the $E_p = 0.2$–0.3 MeV region can be attributed to the excitation of the broad 2^+ state in ^{20}Ne ($E_{cm} = 0.251$ MeV, $E_x = 13.095$ MeV, $\Gamma = 162$ keV [6,33]). The overall forward anisotropy observed at low energies seems mainly due to direct contributions; this point will be examined in detail in a more extended paper.

To obtain the cross section $\sigma(E)$, angular distributions were integrated over 4π. Outside the angular range explored in the present experiment, the angular distribution trend was taken to be the best-fit to experimental angular distributions in terms of 4th order Legendre polynomials. In fact, at these very low energies, only s, p and d partial waves are expected to mainly contribute [9–11]. The astrophysical S-factor is displayed in Fig. 4 (upper panel) as blue dots. The error bars account for statistical errors, while the grey band indicates non-statistical ones. In the same figure results from [9–11] as reported in NACRE [18] are shown as triangles, diamonds and stars, respectively. Empty blue circles show more recent data of Ref. [14]. The green dashed line is the non-resonant NACRE S-factor extrapolation [18]. Present results are in good agreement with the lowermost energy data of [14]. The inspection of Fig. 4 suggests the appearance of several structures as a consequence of the excitation of various resonances in the compound nucleus.

We performed an R-matrix fit of present data and data from Ref. [14]. The E_x, J^π and Γ_{cm} resonance parameters have been fixed from the literature [6,14,20]. As in Refs. [14,20], the high energy part of S-factor data is described by the excitation of the $E_{cm} = 0.801, 0.739, 0.697$ MeV states. The low energy part of data has been reproduced by considering the $E_{cm} = 0.382$ MeV state (3^-, $\Gamma_{cm} = 53$ keV, [20]), the broad $E_{cm} = 0.251$ MeV state (2^+, $\Gamma_{cm} = 162$ keV [6,33]), and the $E_{cm} = 0.204$ MeV state (4^+, $\Gamma_{cm} = 18$ keV, [20]). We included in the fit the $E_{cm} = 0.113$ MeV (2^+, $\Gamma_{cm} = 38$ keV, [20]) state. The resonances at $E_{cm} = 0.113, 0.204$ and 0.382 MeV have been observed with the THM [20] while the resonance at $E_{cm} = 0.251$ MeV was not seen before. We assumed $\Gamma_{tot} \approx \Gamma_\alpha$, which is a good approximation since at energies well below the Coulomb barrier, Γ_p are severely suppressed by penetrability and, consequently, can be neglected in the calculation of the Γ_{tot}. The shape of the non-resonant background has been

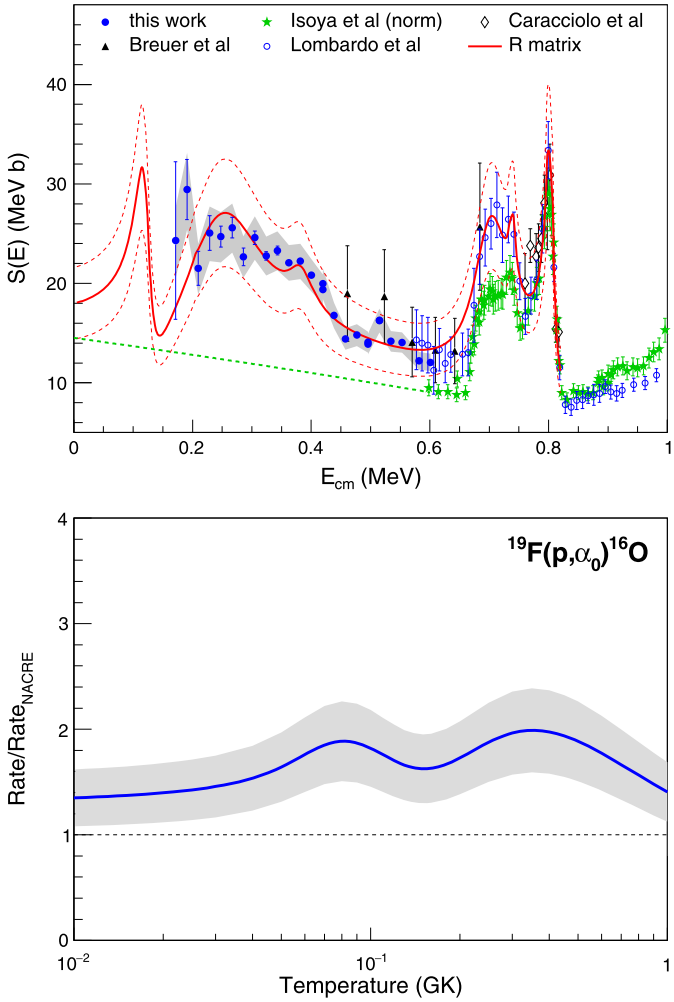

Fig. 4. (Color online.) (Upper panel) S-factor of the ^{19}F(p,α_0)^{16}O reaction at low energies ($\lesssim$1 MeV). Blue solid dots: experimental data obtained in this work (error bars: statistical errors; grey band: non-statistical errors). Black triangles: direct data by [10]. Blue empty circles: data by [14]. Green stars: data by Isoya et al. [9] as normalized by NACRE [18]. Black empty diamonds: data by [11]. Green dashed line: non-resonant extrapolation reported in NACRE [18]. Red line: result of R-matrix best-fit of present data and data by Ref. [14]. White band within the red lines: confidence band of the fit. (Lower panel) Reaction rate calculation (expressed as ratio to NACRE) obtained from the R-matrix fit of the S-factor.

taken from NACRE [18]. The only free parameters of the fit were the scaling factor of the non-resonant background and the Γ_p of the 0.251 MeV state. The result of fit procedure is reported as

red solid line in Fig. 4. The $\widetilde{\chi^2}$ is 0.97 with 36 d.o.f.; the fit describes reasonably well the trend of experimental data in a wide energy domain. The partial widths and, in particular, the Γ_p values are given in [20]. The resonance parameters of the 251 keV peak, not observed in [20], are $\Gamma_\alpha \approx 160$ keV and $\Gamma_p \approx 1.4 \times 10^{-5}$ keV, as obtained from the fit procedure. The scaling factor of the non-resonant background is 1.16 ± 0.04.

The broad bump in the 0.2–0.4 MeV region can be attributed to the constructive interference between the 0.113 and 0.251 MeV 2^+ states superimposed on the direct non-resonant background; the contribution of the 0.382 MeV 3^- state is quite small. We suggest to exclude the opposite interference pattern option (i.e. destructive interference in the 0.3–0.5 MeV region and constructive in the 0.1–0.2 MeV one) because in this case any attempt to better reproduce the experimental trend between 0.3 and 0.6 MeV would result in a worse agreement at energies below ≈0.3 MeV. Indeed, the reduction of the astrophysical factor due to the destructive interference above 0.3 MeV cannot be recovered by increasing the non-resonant contribution, as the fitting curve would dramatically overestimate the S-factor below 0.3 MeV, even taking into account the large errors affecting data in this energy region.

An important resonant contribution from the broad 2^+ state at 0.251 MeV is seen, in agreement with the considerations on the A_4 coefficient made before. In Ref. [20] this state has not been included in the evaluation of the cross section with the THM. Due to the limited energy resolution of the indirect measurement, it was difficult to discriminate the contributions of the 0.204 and 0.251 MeV close lying resonances; considering the poorly known ^{20}Ne spectroscopy in this energy region, at that time the 4^+ 0.204 MeV was assumed to be dominant because of its larger spin, as one can expect from the modified R-matrix formalisms adopted in the THM [20]. Now that these new direct data are available, the authors of [20] started to perform a reanalysis of the indirect data assuming a different level identification, where the 0.251 MeV state plays a more important role. Preliminary calculations show that the THM data can be reasonably fitted by introducing into the modified R-matrix code the 0.251 MeV resonance in spite of the 0.204 MeV one, leaving the same reduced widths as in the present manuscript for the 0.251 MeV state; the parameters of the 0.113 MeV state are in agreement within the uncertainties with the ones of [20]. These aspects will be the subject of future investigations.

The reaction rate calculated by using the R-matrix fit of S-factor data is shown in the lower panel of Fig. 4 (as ratio to the NACRE extrapolation [18]). To evaluate the errors due to ambiguities on the modeling of the non-resonant contribution adopted in the R-matrix fit, we fixed our attention on two different models, the s-wave proton capture estimation used by NACRE (green dashed line of Fig. 4) and the finite-range DWBA calculations of Yamashita and Kudo [28]. If we perform the R-matrix fit by choosing the functional form given by the DWBA model respect to the NACRE one, the resonance parameters remain essentially unaltered, with the low-energy part of the S-factor differing by ≈20% from the fit obtained by assuming the NACRE non-resonant contribution. Taking into account this main source of ambiguity, we conservatively assumed a 20% error level on the S-factor evaluation and therefore on the reaction rate calculation.

On the average, the reaction rate is a factor ≈1.4 larger than the corresponding NACRE evaluation. Local enhancement at $T \approx 0.4$ GK can be mainly attributed to the 0.251 MeV state and its interference with the 0.113 MeV state. The bump at $T \approx 0.08$ GK is originated by the 0.113 MeV state, as seen with the indirect measurement of Ref. [20]. The larger reaction rate observed at temperatures typical of AGB stars should lead to a more efficient ^{19}F destruction by extra-mixing processes. This finding goes in the direction of recent experimental observations of fluorine abundance in metal-poor AGB stars [19,23] and can contribute to solve the puzzle of fluorine nucleosynthesis in AGB stars [34].

4. Conclusions

The present Letter reports new direct experimental measurements of the ^{19}F(p,α_0)^{16}O S-factor at $E_{cm} \approx 0.2$–0.6 MeV. The investigated reaction has a twofold interest: the study of natural-parity states in ^{20}Ne, and the astrophysical implication of the ^{19}F(p,α)^{16}O reaction rate on fluorine nucleosynthesis and CNO cycle. The analysis of angular distribution shapes and the R-matrix fit on the experimental S-factor data allow to determine the contribution given by various resonances (and their interferences) to the S-factor. Present data point out the role played by the 0.251 MeV state (that was not seen with the THM [20] possibly because of its large width) and by the 0.113 MeV state (reported by the indirect experiment [20]). Interference effects between these 2^+ resonances explain the S-factor shape in the 0.3–0.5 MeV region. The reaction rate obtained from the present analysis turns out to be significantly larger than currently adopted low-energy extrapolations. This finding can contribute to solve the puzzle of ^{19}F nucleosynthesis in metal-poor AGB stars by reaction rate reassessments.

Acknowledgements

We are grateful to E. Perillo (Naples) for valuable comments. The continuous assistance of L. La Torre, L. Maran, M. Loriggiola (Legnaro), L. Roscilli (Naples) and Naples mechanical workshop is gratefully acknowledged. We thank F. Camera (Milan) for providing the $LaBr_3$(Ce) detector and G. Imbriani (Naples) for useful discussions.

References

[1] J.D. Cockroft, E.T.S. Walton, Proc. R. Soc. A 137 (1932) 229.
[2] W.E. Burcham, S. Devons, Proc. R. Soc. A 137 (1939) 555.
[3] J.F. Streib, W.A. Fowler, C.C. Lauritsen, Phys. Rev. 59 (1941) 253.
[4] W.B. McLean, A. Ellett, J.A. Jacobs, Phys. Rev. 58 (1940) 500.
[5] R.L. Clarke, E.B. Paul, Can. J. Phys. 35 (1957) 155.
[6] D.R. Tilley, et al., Nucl. Phys. A 636 (1998) 249.
[7] K. Ikeda, N. Tagikawa, H. Horiuchi, Prog. Theor. Phys. Suppl. Extra Numb. 464 (1968) 1.
[8] C. Beck (Ed.), Clusters in Nuclei, Lect. Notes Phys., vol. 818, 2010.
[9] A. Isoya, H. Ohmura, T. Momota, Nucl. Phys. 7 (1958) 116.
[10] G. Breuer, Z. Phys. 154 (1959) 339.
[11] R. Caracciolo, et al., Lett. Nuovo Cimento 11 (1974) 33.
[12] P. Cuzzocrea, et al., Lett. Nuovo Cimento 28 (1980) 515.
[13] S. Ouichaoui, et al., Nuovo Cimento 94 (1986) 133.
[14] I. Lombardo, et al., J. Phys. G: Nucl. Part. Phys. 40 (2013) 125102.
[15] C. Rolfs, W.S. Rodney, Cauldrons in the Cosmos, Chicago Univ. Press, Chicago, 1988.
[16] A. Couture, et al., Phys. Rev. C 77 (2008) 015802.
[17] K. Spyrou, et al., Eur. Phys. J. A 7 (2000) 79.
[18] C. Angulo, et al., Nucl. Phys. A 656 (1999) 3.
[19] S. Lucatello, et al., Astron. J. 729 (2011) 40.
[20] M. La Cognata, et al., Astrophys. J. Lett. 739 (2011) L54.
[21] V.V. Smith, et al., Astron. J. 633 (2005) 392.
[22] K.M. Nollet, M. Busso, G.J. Wasserburg, Astron. J. 582 (2003) 1036.
[23] C. Abia, et al., Astrophys. J. Lett. 737 (2011) L8.
[24] N. Mowlavi, A. Jorissen, M. Arnould, Astron. Astrophys. 311 (1996) 303.
[25] M. Wiescher, J. Görres, H. Schatz, J. Phys. G: Nucl. Part. Phys. 25 (1999) R133.
[26] H. Lorenz-Wirzba, PhD thesis, Univ. of Münster, 1978.
[27] H. Herndl, et al., Phys. Rev. C 44 (1991) R952.
[28] Y. Yamashita, Y. Kudo, Prog. Theor. Phys. 90 (1993) 1303.
[29] C. Spitaleri, et al., Phys. Rev. C 60 (1999) 055802.
[30] A. Couture, PhD thesis, Univ. of Notre Dame, 2005.
[31] J.R. Tesmer, M. Nastasi, Handbook of Modern Ion Beam Materials Analysis, Material Research Society, Pittsburgh, PA, USA, 1995.
[32] G. Raimann, et al., Phys. Lett. B 249 (1990) 191.
[33] C.M. Laymon, et al., Phys. Rev. C 45 (1992) 576.
[34] S. Cristallo, et al., Astron. Astrophys. A 46 (2014) 570.